Effects of dynamics and trigger on energy absorption of composite tubes during axial crushing

Jean-Emmanuel Chambe, Christophe Bouvet, Olivier Dorival, Samuel Rivallant, Jean-François Ferrero

Effects of dynamics and trigger on energy absorption of composite tubes during axial crushing

J.-E. Chambe[a], C. Bouvet[a], O. Dorival[a,b], S. Rivallant[a] and J.-F. Ferrero[a]

[a]Institut Clément Ader, Université de Toulouse, CNRS UMR 5312, INSA/ISAE-SUPAERO/IMT Mines Albi/UPS, Toulouse, France; [b]Icam, Site de Toulouse, Toulouse, France

ABSTRACT

The purpose of this study is to complete a previous quasi-static experimental campaign on the energy absorption performance of composite tubes with the influence of the dynamic effect. Various hybrid composite tubes, involving unidirectional and braided plies with various materials and stacking sequences, were tested both in quasi-static and in dynamic crushing in order to identify their behavior and determine their absorbing capabilities using the Specific Energy Absorption. In dynamic loading, 90°-oriented fibers stabilised by woven plies showed good performances, contrary to static loading, since the energy absorption of the unidirectional laminate oriented at 0° drops by 50% in dynamics.

KEYWORDS

Dynamic crushing; composite tubes; energy dissipation; specific energy absorption; crash; aeronautics

1. Introduction

Performances of shock absorbers are of paramount importance [1–3], as human tolerance and crash survivability are utterly dependent on the energy absorbing parts positioned within the transportation structure. The purpose of those parts is to reduce the loads or accelerations induced during the crash by absorbing the crash energy. In homogeneous metal systems, energy is absorbed by plastic dissipation, and optimization of shock absorbers requires to 'trigger' local modes of deformations, for instance by weakening some zones by groove patterns [4] or using sine shaped structures [5]. In composite structures, triggering of local modes of deformation is inherent to the material inhomogeneity and optimization of the energy dissipation needs to capture the good rupture mechanisms. Many studies regarding composite structures crashworthiness and inherent energy absorption capabilities have been carried out under quasi-static loading conditions. However to fully apprehend the crash aspect, automobile impact and aircraft crash must be considered as dynamic events, thus involving high velocity [1].

Composite materials are perceived as potential component for high energy absorption due to their low density combined with strong mechanical properties. Their ability to dissipate energy is mainly due to the highly dissipative rupture mechanisms involved during the severe solicitations [6–9] underwent in crushing. Successive stages of progressive crushing of a composite tube have been well identified [10–12] in quasi-static loading, see Figure 1: elastic loading (a), rupture initiation at peak loading (b) followed by a sudden load drop (c, d) and a constant plateau (e, f) named progressive crushing plateau. During a progressive crushing mode (see Figure 2 from [10]), rupture mechanisms at the structural scale may be summed up into three types: (i) splaying, (ii) fragmentation and (iii) debris creation and accumulation [10,13,14]. Predominant rupture that leads to the structure yielding and energy dissipation includes quasi-brittle fracture and delamination combined with transverse tearing and kink-band formation [15,16].

Optimization of composite shock absorbers then requires to investigate the parameters of the composite structure (materials, stacking sequence and composite nature) and that of the shock absorber itself (structure shape and dimensions, material orientation to the load, and trigger for instability initiation). The difficulty lies in two reasons: the first one is the fact that all these parameters are interdependent, the second is that dynamics is likely to provoke changes is the deformation and as a consequence in the absorption performances of the structures.

The following main tendencies tend to stand out in quasi-statics, see the review by Mamalis et al. [9], but dynamic aspects still raise some discussions in the scientific community:

- In the field of shock absorption, tubular structures with various cross-sections have received particular attention. Most studies find the energy absorption capability of squared tubular structures to be 0.5 times lower than that of circular ones under axial crushing. Thornton et al. [17] stated that the specific energy absorption of fabric lay-up tubes increases in the following order for a given size: rectangular < square < round. In case of tubular structure, the tube thickness [18–23], or the diameter to thickness ratio [22,24,25] have also been investigated.

CONTACT C. Bouvet christophe.bouvet@isae-supaero.fr

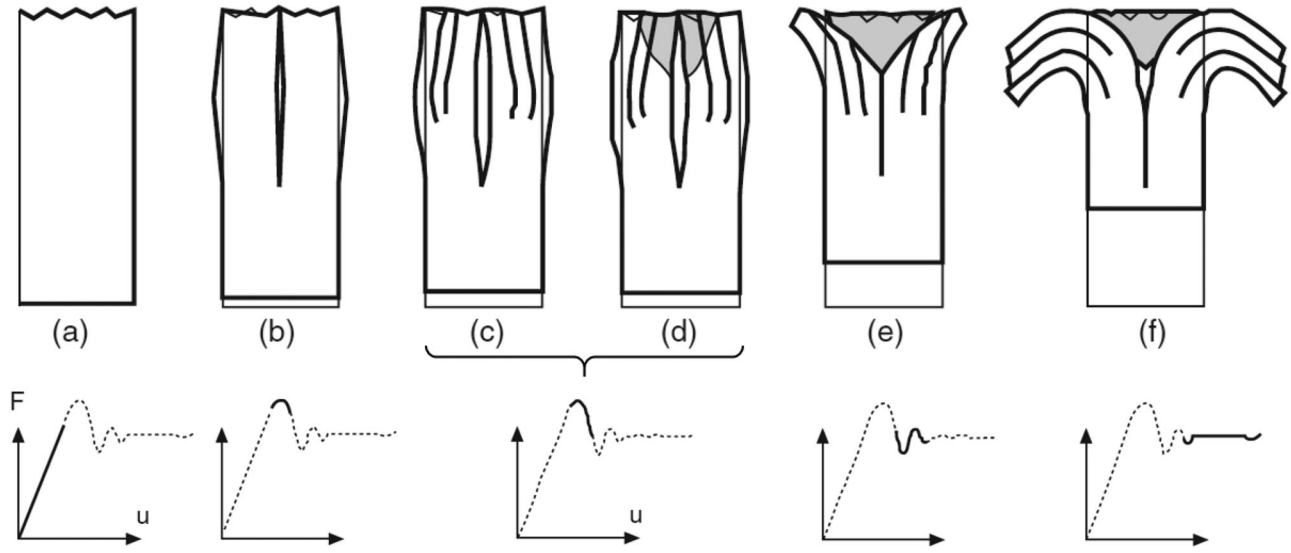

Figure 1. Consecutive crushing stages (adapted from [11]).

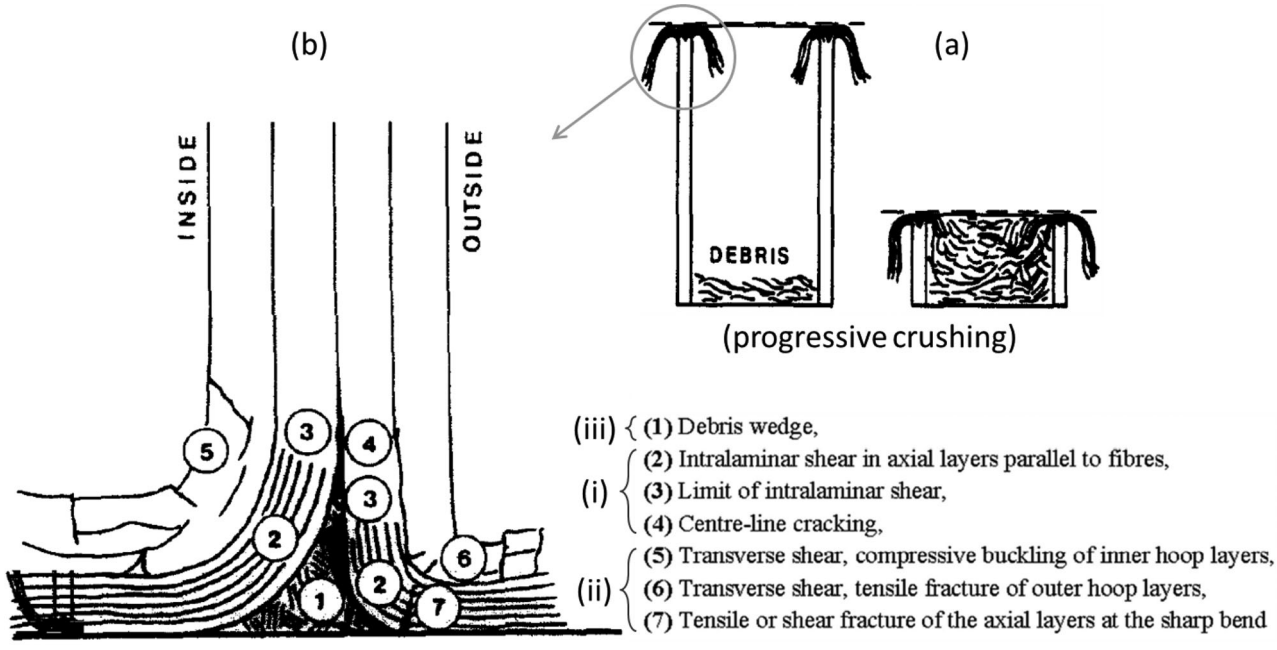

Figure 2. Major rupture mechanisms occurring at the crush zone (adapted from [10]).

- Numerous investigations have been carried out on the choice of composite materials, mainly FRP [17,24,26] with a various range of fibers, such as carbon, glass and aramid, and with various resins. Browne et al. [18] reported a 20% to 62% increase using unidirectional carbon fibers tow with adjacent oriented fabric plies compared to aluminum construction, with an average SEA value of 32.5 kJ.kg^{-1}. Carbon/PEEK [8,27] and carbon/epoxy [1,13,14,18,26–43] have been reported as the most performant materials combination in term of energy absorption by most of the studies. The effect of the laminate type, involving either unidirectional plies (UD) [1,14,28,31,32,39,44], 2D-braidings or 3D-braidings [13,18,22–47] have also been largely tested. In general, it was observed that the tri-axially braided architectures perform better than the bi-axially braided type or UD type.
- Among others, Chiu et al. [28] proposed some insights in the rupture initiation of axial crushing of tubes regarding ply orientation with respect to that of the load. In the 0° plies, where the majority of loading is borne by the fibers, the main form of damage is large brittle fiber breakage along vertical matrix shearing. Conversely, in the 90° plies, the predominating damage mode is shear matrix cracking in a direction parallel to the fibers, incidental with limited fibers breakage. The shear cracking is likely triggered by the compressive loading transverse to the ply.
- Improving the crushing initiation with specific trigger systems has been widely attempted in order to favor the

desired crushing mode, using different trigger profiles [43,48], via chamfered or beveled edges [7,13,14,18,20–42,45,49], and also with the presence of a plug initiator [13,20,34,38,43,46] to enhance the crushing. Although not always consistent in terms of SEA levels being reached, all studies concur in finding a strong plug-initiator influence on the crushing performances, what usually corresponds to a SEA decrease in the presence of a plug initiator. Chamfered-edge tubes produced the best results in term of initiation and energy absorbing capacity according to Brighton et al. [13], but the use of a plug initiator tremendously reduced the SEA [13,46]. Furthermore, regarding the size, tallest plugs most reduced the SEA capacity according to [13]. Moreover, concerning such plug initiator triggers, it has been reported that the plug radius has a strong effect, with an energy absorption capability that decreases all the more as the radius is important [13,20] compared to none radius plug. The SEA level has been found to drastically decrease with the increase of the plug size (see Table 2).

It is important to stress the influence of dynamics. Although there is not always a clear consensus whether dynamics change the deformation mode, almost every instance from the literature reports a strong to moderate decrease in energy absorption capacity from quasi-static to dynamic loading for fiber-reinforced composite materials (see Table 1). Contrary to other results in literature, Muralikannan et al. [22] reported that the basic modes of deformation for tubular structures are the same for both quasi static and dynamic loading. For Brighton et al. [13] SEA values of carbon/epoxy tubes decreased for increased testing speed, specifying that the 45° chamfer carbon/epoxy tests showed the highest SEA and the least dependence on loading speed [13]. A notable decrease was also observed by McGregor et al. [46] in dynamic loading when using a plug initiation form. Numerous studies focused on the strain rate or velocity effect [1,7,13,17–29,31,39,41,42,45–47] with many performing a quasi-static/dynamic comparisons [7,13,19,21–42,46,47,49]. Most studies concurred and highlighted a velocity dependence, finding a moderate to substantial decrease in SEA values from quasi-static to dynamic loading [13,19,22,23,27,33,39,42,46], with a 12 to 33% decrease on average. Some examples are reported and synthetised in Tables 1–3.

Focusing on the material type, Schmueser and Wickliffe [19] reported a decrease in energy absorption of dynamic impacted carbon/epoxy, glass/epoxy and kevlar/epoxy tubes as compared to quasi-static loading. With the ply orientation taken into account, Farley [31] found no difference between low and high velocity, reporting that specific energy absorption is independent of crushing speed for 0°+oriented structures (labelled [0°±θ]). However, the author remarked an increase in energy-absorption capability for pure [±θ] structure, reporting the magnitude change to be a function of the ply orientation (±45° and ±75° in his study). David et al. [39] found similar results for pure [±θ] structure (at ±45°) hence joining Farley [31] on crushing speed and orientation dependence. Schutlz et al. [33] however, despite reporting a clear energy absorption drop between dynamic and static testing, reported only a very slight but not significant nor constant lay-up and fibers orientation influence. The effect of fibers orientation and the presence of 0° unidirectional plies in the lay-up structure appeared to have a limited influence since reported performances are not repeatable from one sample type to another and the effect of unidirectional plies is not observable on some samples.

Table 3 reports synthetised results from previous studies on the influence of fibers orientation and structural lay-up on the SEA values between quasi-static and dynamic loading.

When so many parameters are found to have a strong influence, and no clear conclusions can be drawn from literature review, numerical modeling may be a valuable solution to optimise the parameters. However dealing with such complex damaged mechanisms encountered in axial crushing of tubes is not straight forward as it requires experiments for model calibration. The current paper aims at comparing the results in energy absorption capability of hybrid composite circular structures with different fibers orientations and of different natures (UD, woven) using specific boundary conditions and trigger initiation systems in both quasi-static and dynamic crushing. Only one impact velocity is being tested in the present work. The work presented in this study is a key step toward the development of robust numerical models.

The paper is organised as follows: Section 2 describes the materials tested and the experimental set-up and methodologies. Section 3 presents the experimental results in terms of peak stress, mean stress and SEA comparisons. Some conclusions are drawn in Section 4.

Table 1. Variation of SEA values from quasi-static to dynamic crushing.

	Variation from quasi-static to dynamic loading
Schmueser and Wickliffe [19]	−13%
Mamalis et al. [23]	From −11% to −33%
Schultz et al. [33]	From −14% to −32%
Brighton et al. [13]	From −13% (chamfered) to −20% (with plug)
David et al. [39]	−23%
McGregor et al. [46]	From −35% (without plug) to −51% (with plug)
Hu et al. [42]	From −12% to −32%

Table 2. Comparison of SEA drops in dynamic crushing due to boundary conditions.

	Variation in dynamic loading
Brighton et al. [13]	Plug size (height) down to −55%
McGregor et al. [46]	Plug initiation from −23% to −32%

2. Experimental testing

2.1. Specimens and materials

A variety of fiber/epoxy tubes were acquired for testing, with different fibers orientations and fibers types. These fiber-reinforced tubular structures were studied in axial compressive crushing, at two different rates, namely quasi-static and dynamic. In total, five specimens with different structures and different compositions were tested in various crushing configurations. Structural and material basis for the

Table 3. Variation of SEA from quasi-static to dynamic for different fibers orientations.

		Variation from quasi-static to dynamic loading and dependence on fiber orientation		
Farley [31]	[0° ± θ]	No effect	[±45°][±75°]	+41% to 61 kJ/kg
David et al. [39]	[0/90°]	−23%	[±45°]	+12% to 77 kJ/kg

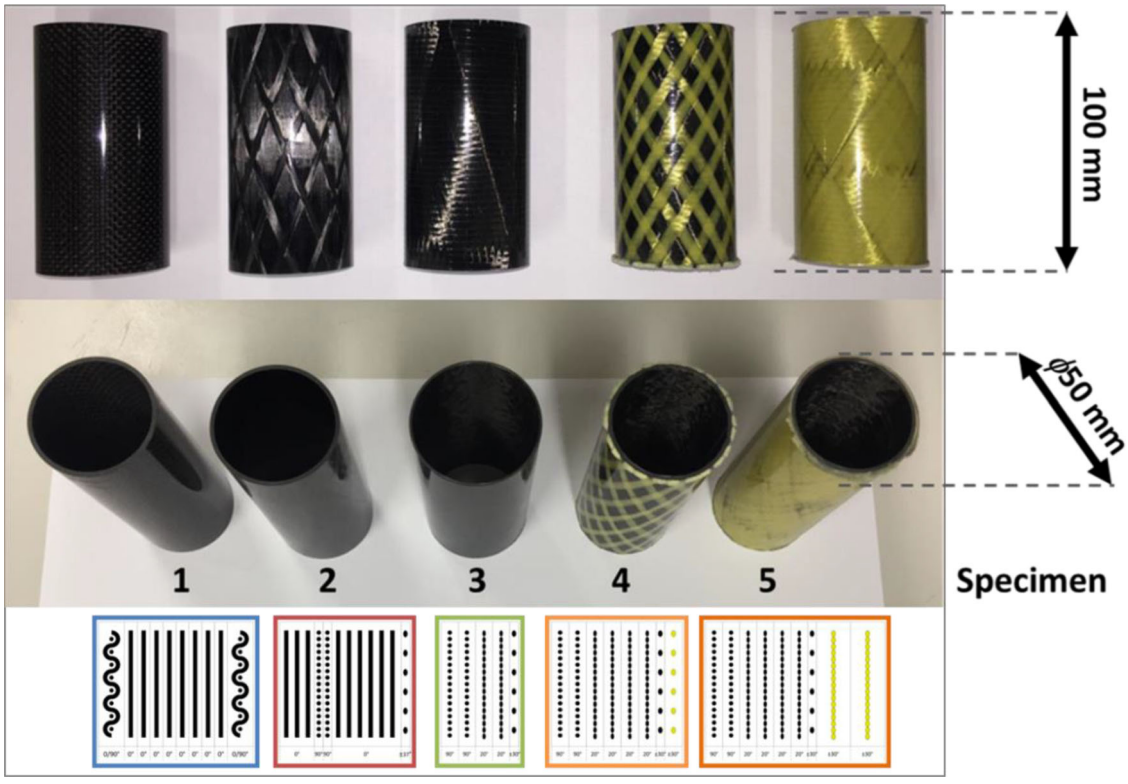

Figure 3. Photos and drawing of the five tube specimens with dimensions.

specimens include 12 K HR carbon fibers and polymer epoxy resin. Fibers orientation and laminate stratification differ from one specimen to another as shown in Figures 3 and 4 and summarised in Table 4. Provided tubular structures were machined and shaped in tubes of 100 mm length as pictured in Figure 3. Medium diameter was set at an average of 50 mm, with inner diameter varying from one sample to another due to stacking differences. Stratification layout and tube wall thickness are summarised in Table 4 for each sample.

The carbon/epoxy combination was selected with epoxy resin as a matrix because of its low density and for its high strength and good mechanical properties with reliable chemical stability, as well as its worthy performance regarding energy absorption based on the literature review and due to the aeronautical context.

In order to verify and establish the composition and stratification of the composite tubes specimens, samples were polished and observed using a high resolution optical microscope. Measurements and images acquisitions were performed using an Alicona Infinite Focus SL microscope system with a x10 to x50 magnification. Resulting observations are displayed in Figure 4, along with a lay-up schematization.

For the laminate lay-up schematization presented in Figure 4, the 0° direction of the fibers was chosen to coincide with the longitudinal axis of the tube and subsequently with the axial crushing direction. Plies dimensions are given as an averaged best approximation since plies thickness is not even and regular. That is supposedly the results of the fabrication process.

Table 4 reports the structural specificities and geometrical properties for the five tube specimens.

Table 4 presents the stratification structure in number of plies. The 'individual' thickness of the plies (or group of plies) is given in Figure 4.

When looking at the density values from Table 4, it can be pointed out that they are relatively low for some samples (sample 1 especially, and to a lesser extent, sample 3). This is allegedly strongly related to the high porosity observed in the samples (see Figure 4) and also lower fiber density (or fraction volume v_f) in some areas of the samples.

For the five tubular specimens (and especially for tube samples 1 and 2) materials and fibers properties are not well known and identified nor completely mastered. Preliminary compressive experimental testing shows that fibers mechanical properties are less resistant than usually encountered in current modern composite materials.

In order to better estimate the mechanical properties of the materials used to manufacture these samples, and to correlate the theoretical and experimental stiffness, Classical Laminate Theory (CLT) was used. Taking a failure criterion

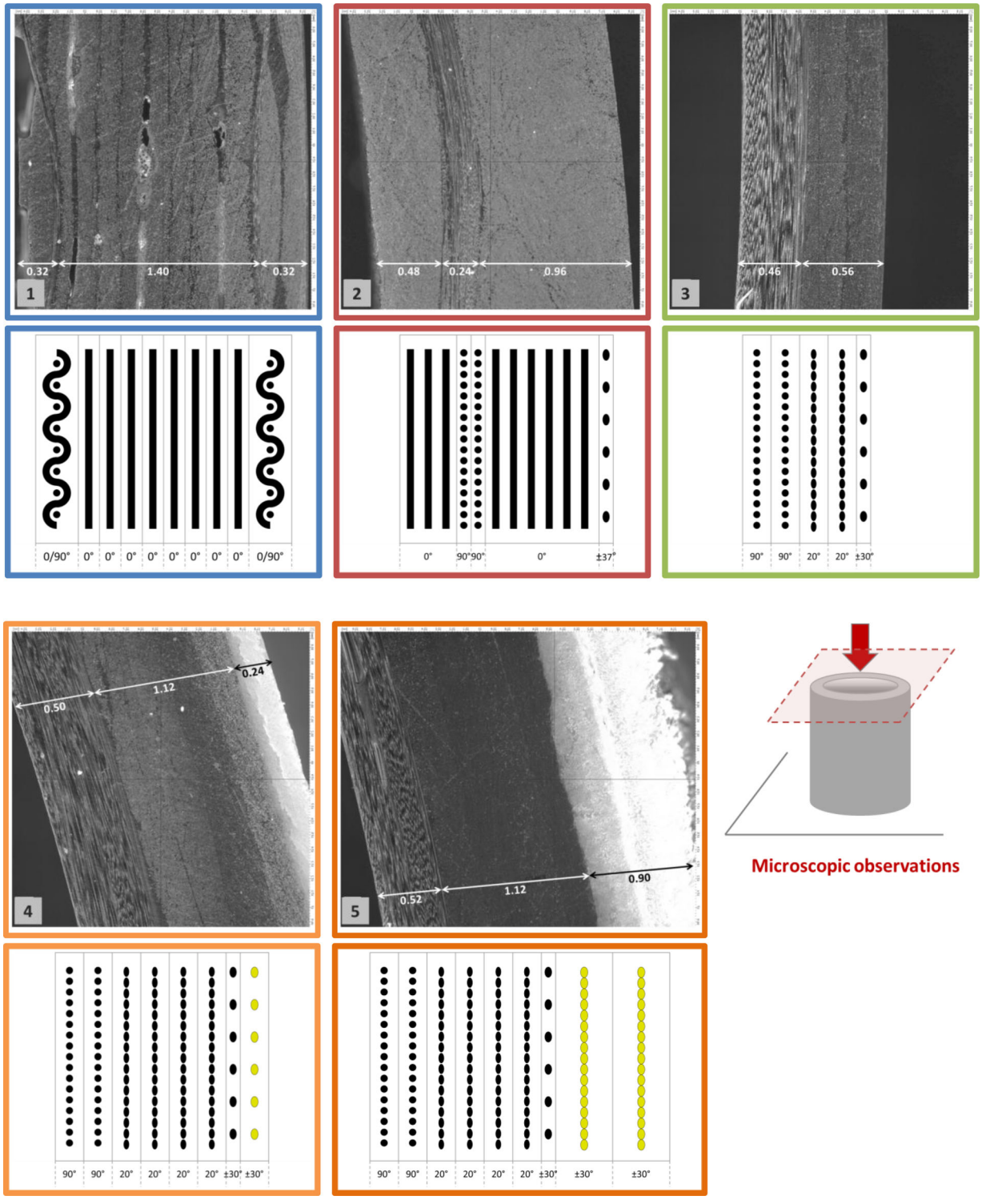

Figure 4. Microscopic observations of the five specimens section and corresponding schematic representations of the stratification.

expressed in fibers compression strain, chosen at $\varepsilon_{failure} = -0.0125$ for all the plies, an estimated stress failure value was calculated for each sample, for the first ply reaching $\varepsilon_{failure}$. For the woven plies of the structures, mechanical properties were also calculated using the CLT but the related plies were approximated as two superposed oriented unidirectional plies of half the thickness. The mechanical stiffness properties used for the theoretical calculations with the CLT are reported in Table 5, where E_l is the longitudinal modulus, E_t the transverse modulus, G_{lt} the shear modulus and ν_{lt} Poisson's ratio. Calculated theoretical values are reported Table 6.

Table 6 intends a comparison in stiffness and compressive strength failure between experimentally and theoretically obtained values for all five samples. Both the experimental and theoretical methods used to achieve those

Table 4. Tubes specimens stratifications and properties (C: Carbon A: Aramid).

Ply\Tube	Specimen 1		Specimen 2		Specimen 3		Specimen 4		Specimen 5	
1 (inner ply)	0/90° (weave)	C	0°	C	90°	C	90°	C	90°	C
2	0°	C	90°	C	90°	C	90°	C	90°	C
3	0°	C	90°	C	20°	C	20°	C	20°	C
4	0°	C	0°	C	20°	C	20°	C	20°	C
5	0°	C	±37° (weave)	C	±30° (weave)	C	20°	C	20°	C
6	0°	C					20°	C	20°	C
7	0°	C					±30° (weave)	C	±30° (weave)	C
8	0°	C					±30° (weave)	A	±30° (weave)	A
9	0°	C					(30% cover)		±30° (weave)	A
10 (outer ply)	0/90° (weave)	C							(100% cover)	
Wall thickness (mm)	2		1.8		1.1		1.85		2.45	
Int. diameter (mm)	46		46.5		50		45		45	
Ext. diameter (mm)	50		50		52		48.5		49.5	
Density (kg/m^3)	1.34E + 03		1.69E + 03		1.43E + 03		1.50E + 03		1.39E + 03	

Table 5. Mechanical properties used for the classical laminate theory calculations.

	E_l (MPa)	E_t (MPa)	G_{lt} (MPa)	ν_{lt}
Carbon				
UD	62,000	7700	4200	0.25
Woven	35,000	35,000	4200	0.05
Aramid				
UD	61,000	4200	2900	0.35
Woven	30,000	30,000	2900	0.30

results are presented below. The magnitude referred to as stiffness (in MPa) relates to the elastic compressive modulus (Young's modulus).

When comparing values from the theoretical calculations to the experimental data (Table 6), the latter reflects lower values in stress failure, although it can be noted that they remain in the same order of magnitude. Moreover, the experimental compressive strength values that are reported in Table 6 are rather related to a failure in crushing mode than pure compression, which can further explain the observed differences.

Results reported in Table 6 show that the compression stiffness is lower than anticipated for three of the five CFRP specimens, especially for specimens 1 and 3. Compression failure is also lower than estimated, especially for specimens 1 and 2 that incidentally mainly present 0°-oriented fibers.

This supports the hypothesis of poor fibers properties used to manufacture the tubular specimens, and it can also be explained by the high porosity inherent to many samples, as observed on the microscopic images (see Figure 4). This is also most obvious for tube specimen 1, for which braided thread remnants from the manufacturing process are visible too. In addition, experimental compressive failure values resulting from the performed compression tests could rather be affected by a bearing phenomenon under the tip of the plies and resulting from the crushing nature of the solicitation than related to a pure compressive mode, hence the observed discrepancy in compression strength failure, which thereafter seems more rational.

2.2. Test set-up and configurations

With the objective of establishing a comparison, both quasi-static and dynamic testing were carried out for the purpose of this study.

Quasi-static crushing tests were carried out using a 250 kN Schenck hydraulic testing machine in compression testing mode, through a constant loading speed of 0.2 mm.s^{-1} (see Figure 5). To account for repeatability, tube specimens were tested at least 3 to 5 times on average for each sample and each configuration. More details on experimental testing conditions and results can be found in a companion paper (see [50]).

Dynamic shock testing trials were carried out using a drop tower shown in Figure 6. The apparatus pictured in Figure 7 both allows to easily change configuration and to protect the sensors in case extra energy needs to be absorbed. Load and displacement were acquired during testing and trials were monitored using rapid imaging cameras. To monitor the trials and verify that the velocity did not intensely decrease during mass dropping due to friction or out of alignment fall, a high-speed camera FastCam Photron SA5 was employed to record trials pictures at high speed with 20 000 FPS.

Specifications for the drop tests were:

- drop mass: 215.5 kg
- drop height: 1.25 m
- corresponding to a theoretical speed at impact of: 4.95 m.s^{-1}, or 2.64 kJ input energy.

Figure 7 presents a detailed schematization of the experimental set-up assembly for the different configurations tested, corresponding to different boundary conditions and trigger systems.

In this experimental set-up, a mobile mass is dropped from a predefined height on a stacking of several components. From top to bottom, they consist of the studied composite tube sample, encased on the top end and positioned on one of either three different parts (see Figures 6–8), setting the boundary conditions for the trials. Three load sensors are then equidistantly positioned, in a 120° triangle shape between two steel reinforced plates. The sensors are fixed between the plates using through screws and are slightly pre-stressed. Finally a Nomex®/or aluminum honeycomb absorber brick is placed underneath the assembly in order to dissipate any residual energy that would not have been absorbed by the composite tubular

Table 6. Stiffness and compressive strength properties for tube specimens 1 to 5.

	Experimental				Theoretical	
	Stiffness (MPa)		Compressive strength (MPa)		Stiffness (MPa)	Compressive strength (MPa)
Tube 1	43,700	+2800 −5200	350	+100 −139	54,200	650
Tube 2	54300	+4900 −3100	340	+65 −102	52,100	652
Tube 3	30,200	+8700 −8600	170	+47 −92	22,800	265
Tube 4	27,300	+6800 −6000	180	+44 −59	24,500	259
Tube 5	24,700	+3600 −5400	200	+29 −41	23,600	250

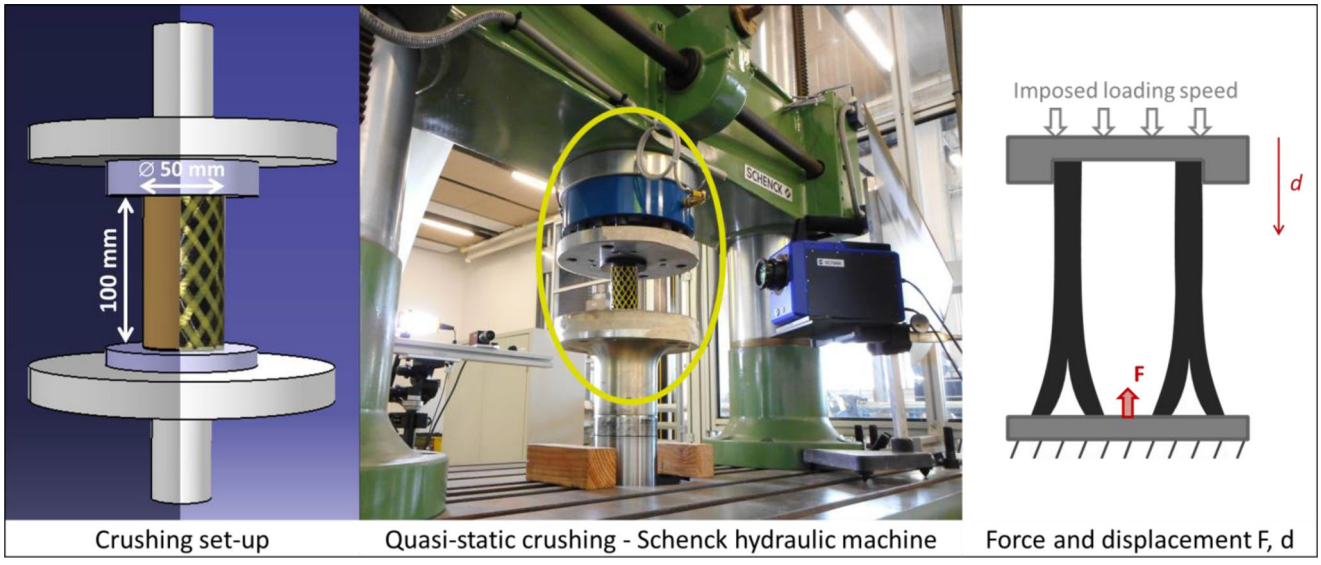

Figure 5. Quasi-static crushing test set-up and equipment.

structure during crushing. Adjustment wedges were used as drop-mass stops to prevent tubes specimens from totally collapsing and preserve the integrity of the assembly underneath.

Tubes specimens 1 to 5 were tested in three main configurations denoted by (a), (b) and (c) and detailed in Figure 8 with a focus on tube 1 and 2 in configuration (b) and (c), which produced the best results in quasi-static crushing. Tube specimen 3 was only tested in configuration (a) and (b) and tubes specimens 4 and 5 were only tested in configuration (a), as a consequence of the available quantities of materials. To account for the repeatability, tests were performed one to three times depending on the configuration and materials (number of tube specimens) availability.

For the inner conic configuration (c), forcing a compressive hoop strain of -0.015 def, the diameter of the base of the conic-shaped part (d_{ext}) was made to match the exterior diameter (Ext. diam.) of the tube. Specifications are reported in Table 7. The same conic part was used for tube specimens 1 and 2, as they have similar diametric dimension (especially the exterior diameter). As a reminder, tube specimens 3 to 5 have not been tested in this particular configuration.

2.3. Post-processing methodology

The beginning of the test is defined at $t_0 = t_{impact}$, the time when the mobile mass reaches the sample and impacts the upper part of the experimental configuration clamping the tubes.

Raw data acquired from the 3 HBM C6A (200 kN) sensors is summed and converted to kN and then filtered in order to be able to compare dynamic results with quasi-static results. As an example, Figure 9 presents the stress and stress-filtered (*) data for tube specimen 1 in inner crushing configuration (b).

In order to have a better reading of the signal, the force and stress signals resulting from dynamic trials were filtered using a time-dependent filter as described below (Equation (1)):

$$x^*_{n+1} = \alpha\, x_{n+1} + (1-\alpha)\, x^*_n \quad (1)$$

with x_n value at n of the original signal;

x^*_n value at n of the filtered signal.

and $\alpha = 2\ \Delta t\ f_0$ with Δt the time interval between x_{n+1} and x_n and f_0 a cutoff frequency, taken at 2 kHz.

This cutoff value was chosen in adequacy with the resonance frequency of the sensors (4.5 kHz) and in order to

obtain trend curves more easily comparable to quasi-static curves results. Besides providing a clearer signal and offering a better interpretation, dynamic signals filtering helps with the comparison between quasi-static and dynamic testing.

Figure 6. Photo of the drop tower testing equipment. The zone boxed in blue shows the sample and the interface parts (see details in Figures 7 and 8).

One drawback from filtering, however, is that the filtered signal is heavily dependent on the filtering parameters. The overshoot factor, which may be defined by the crushing stress initial peak maximum value divided by the density (Equation (2)), is a useful indicator chosen to represent and compare the overflow of energy. As this factor is uniform to the SEA ($kJ.kg^{-1}$) a direct comparison between these two values is usually possible during a quasi-static approach. In dynamics, signal filtering strongly interferes with the initial peak load and therefore any attempt to properly evaluate the overshoot (see Equation (2)) is improper. As an example, the filtering influence over the overshoot is clearly visible and displayed in Figure 9, where both signals are overlaid.

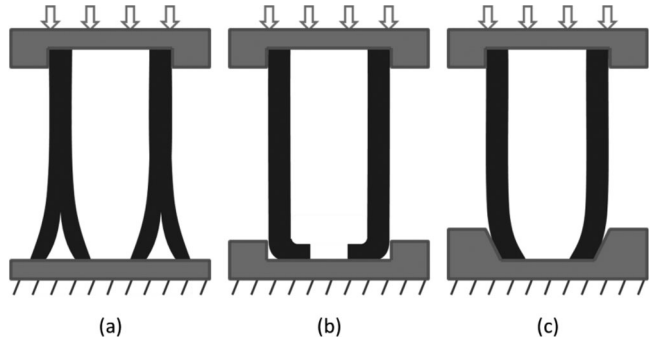

Figure 8. Experimental testing configurations: free crushing (a), inner crushing (b), inner conic crushing (c).

Table 7. Inner conic part dimensions for configuration (c).

Tube	Specimen 1	Specimen 2
Int. diam. (mm)	**46**	**46.5**
Ext. diam. (mm)	50	50
Inner cone (15,000 μdef)	Inner cone 1	Inner cone 1
Inner cone D_{ext} (mm)	52	52
Inner cone d_{ext} (mm)	49.3	49.3

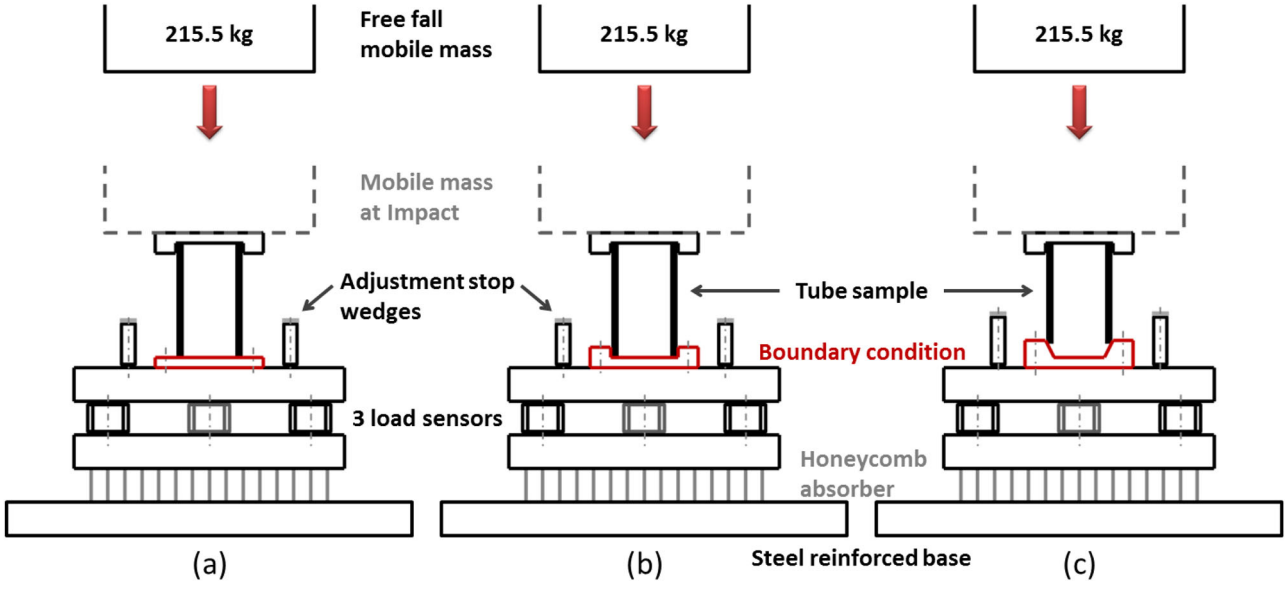

Figure 7. Dynamic shock testing system configuration (a), (b), (c) (see details in Figure 8).

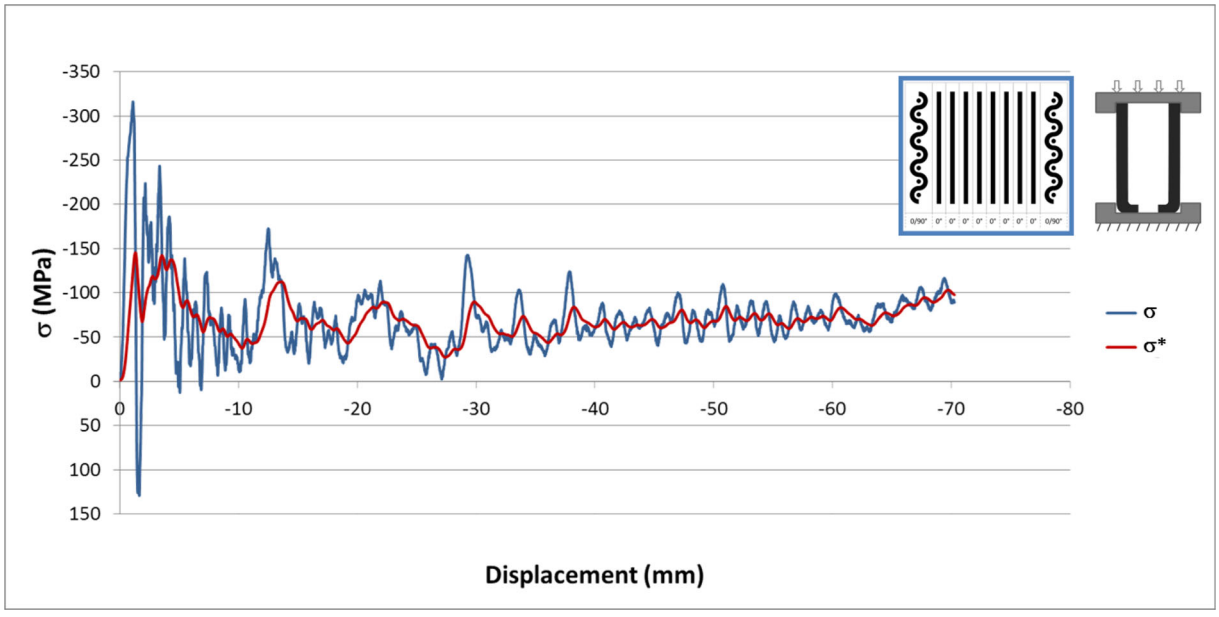

Figure 9. Stress and stress-filtered (*) curves over displacement (blue and red, respectively) for tube specimen 1 in the inner crushing configuration (b).

$$\text{overshoot} = \frac{\sigma_{max}}{\rho} \quad (2)$$

2.4. Specific energy absorption and overshoot

One means to characterise and compare the absorbing capability of materials is through the Specific Energy Absorption (SEA), also referred to as Specific Sustained Crush Stress. The SEA value is given by the following equation (Equation (3)):

$$SEA = \frac{EA}{m} = \frac{1}{\rho\, u}\int_0^U \sigma(u_z)du_z \quad (3)$$

with:

EA is the energy absorbed,
m is the mass of the crushed mater,
ρ is the density of the material,
u is the crushing distance,
σ is the compression stress.

As the initial peak quickly drops to a crushing plateau, a very reliable approximation of the SEA value can be obtained 'instantaneously' using the stabilised crushing stress σ_{cr} (in MPa) divided by the density ρ of the crushed material (Equation (4)):

$$SEA\ \sigma \rightarrow const\ \frac{\sigma_{cr}}{\rho} \quad (4)$$

The SEA consideration as a mean to evaluate the energy dissipated presents the tremendous advantage of easily and directly comparing different materials energy absorption capacity as it is directly linked to their crushing performance and takes into account their inherent density.

In order to quantify the efficiency of a shock absorber, the load efficiency ratio is often used, and is defined as the ratio of the plateau crushing force to the initial peak force. Optimum shock absorber has a ratio of 1 that traduces a perfect plastic behavior. Another way of estimating the efficiency of a shock absorber is to use the overshoot (see Equation (2)) that has the advantage to have the same unit than SEA. Direct comparison between overshoot and SEA shows the 'drop' in efficiency for a given structure. The same value for overshoot and SEA is the perfect plastic case that is the optimal shock absorber.

3. Experimental results

3.1. Crushing stress signal

Similar to what is observed in quasi-static crushing tests, the stress signal in dynamic loading also decomposes in three stages: a loading phase ending by the main rupture of the structure and leading to an initial peak load, a stabilization phase and a stable crushing phase, as previously reported in many studies [10,12] and observed in Figures 9 and 10. Occasionally, if crushing is prolonged long enough, a last phase known as compaction of debris or densification may occur, matching an increase of the stress curve at the end.

Figure 10 depicts a typical stress-displacement curve for a dynamic crushing trial, using tube specimen 1 in configuration (b) (inner crushing) as an example. The stress value results from the summation of the data acquired by the three load sensors evenly positioned beneath the tested structure (see Figure 7). More oscillations are observed in dynamic loading than in quasi-static (see Figures 10, 13 and 15) because of a shock wave effect, generating a rebound in the impacted structure as well as back and forth waves within the drop test system. Also, due to the current testing configuration, the sensors position is slightly distant from the impact area, marginally impacting the signal.

Generally, a relatively good repeatability can be noted in the dynamic testing from one trial to another, especially considering the dynamic and composite material factors, as illustrated in Figure 10, with a dispersion range of -24% and +35% compared to a medium value, resulting from an averaging of all trials data in this configuration. The dispersion

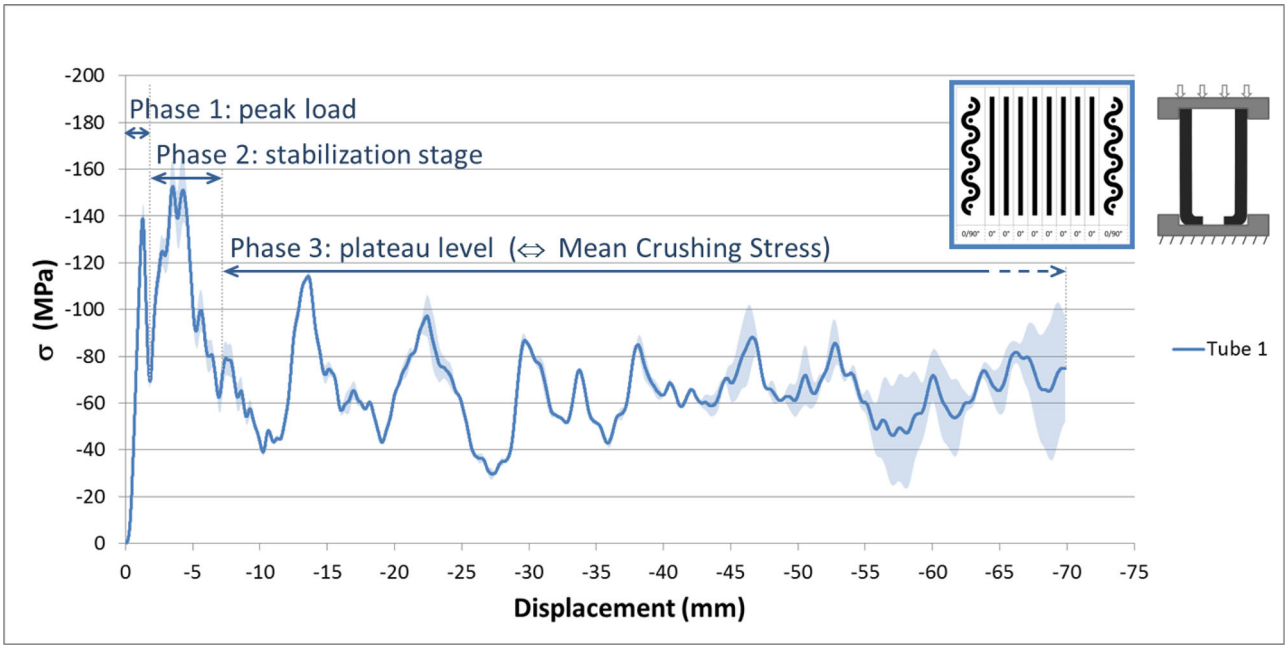

Figure 10. Stress-displacement curve and dispersion for tube specimen 1 under crushing.

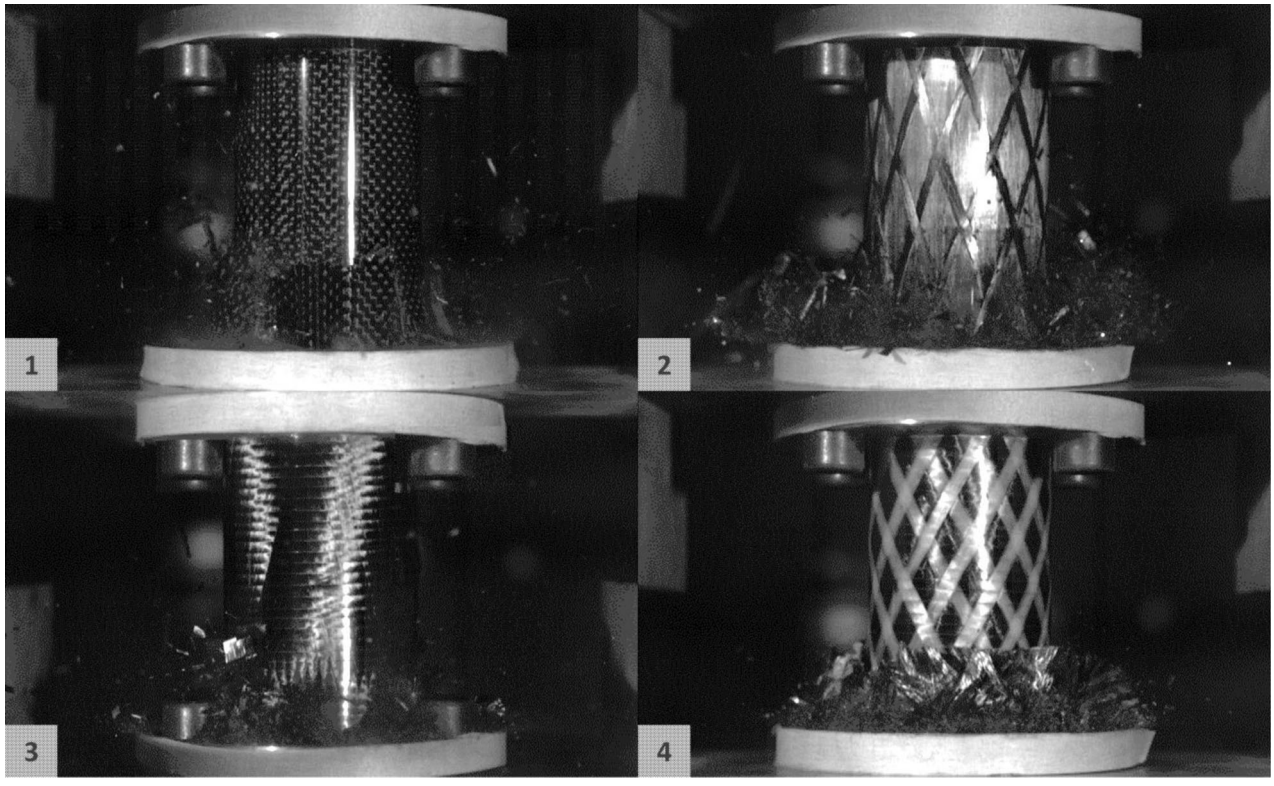

Figure 11. Dynamic crushing of tubes samples 1 to 4 in free-crushing configuration (a).

area on this graph is obtained using a superimposition of the lowest and highest curves results for this trial. Overall, less than 1% of the total of tested samples has been discarded by being deemed aberrant.

Photographs presented in Figure 11 display a snapshot of crushed CFRP tubes for samples 1 to 4 in free crushing configuration (configuration (a)) recorded by rapid-imaging camera. Brittle fracture and debris generation are clearly visible for tube samples 1, 2 and 3, whose reinforcement is constituted of pure carbon fibers, unlike what can be observed for tube samples 4 and 5, where the aramid cover acts as a girdle, drawing the shattered composite fronts, resulting in a close folding and wrapping around itself. This aramid net therefore helps with debris containment and refrains large outer spreading. Tube sample 5, although not displayed in Figure 11, behaves very similarly to tube sample 4.

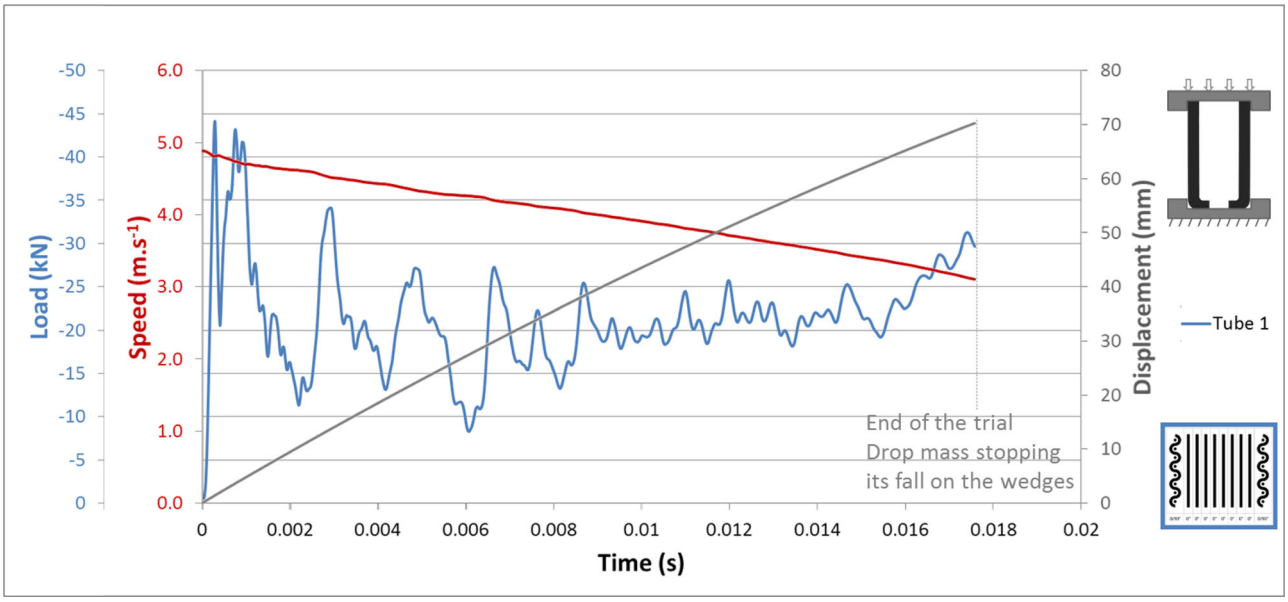

Figure 12. Speed, displacement and load versus time for tube specimen 1 under crushing.

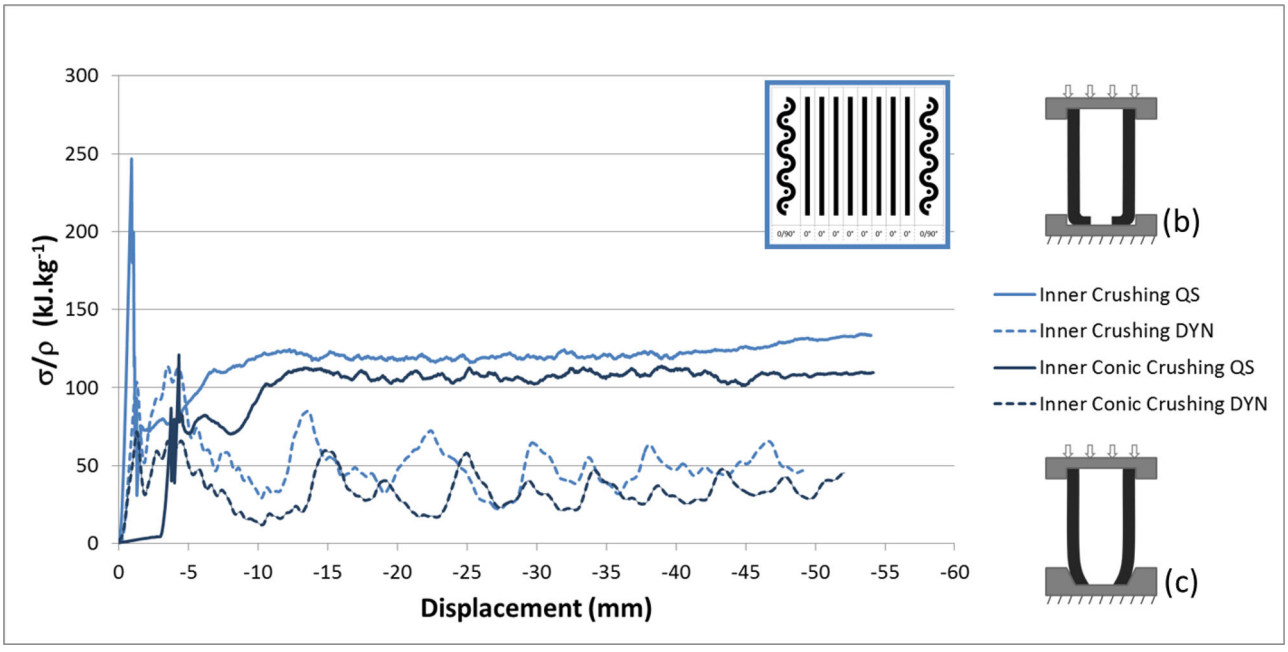

Figure 13. Stress over density/displacement curves for tube sample 1 in configurations (b) and (c).

During such dynamic crushing tests, i.e. using a mobile drop mass, the speed of that mobile mass decreases as it crushes the impacted sample, from contact at t_{impact} to the end of the test, as can be observed in Figure 12, displaying the load (blue) registered by the sensors during the crushing of tube specimen 1 in configuration (b), with the corresponding speed (red) and displacement (grey). The speed of the drop mass (red) decreases linearly as the displacement (length of the tube being crushed) increases progressively (grey). They both end their progression when the mobile drop mass is stopped by the lateral wedges. The speed presented in Figure 12 results from a first integration of the motion equation of the drop mass, and the displacement from a second integration.

3.2. Crushing stress and testing configurations

This section discusses the stress over density (σ/ρ) curves for different tubes samples and compares different testing configurations in quasi-static and dynamic loading. Composite crushing in dynamic loading significantly reduced the stress generated and thus the SEA values, compared to quasi-static crushing of the same

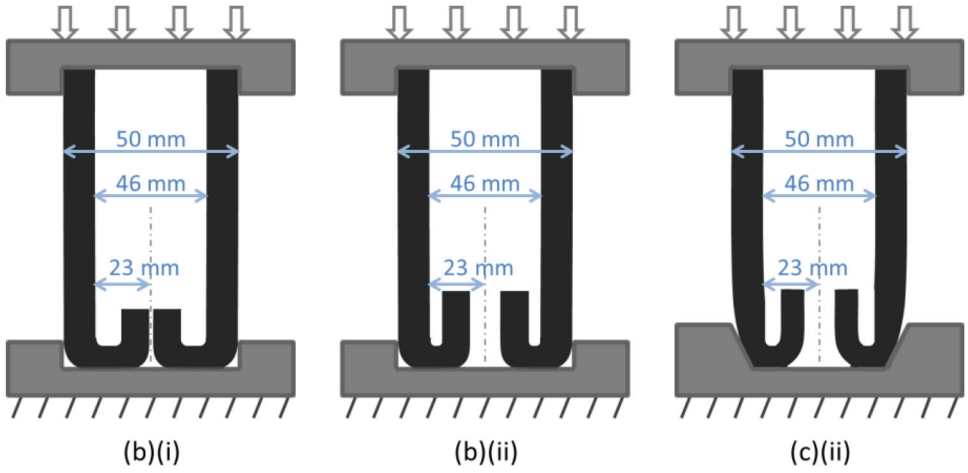

Figure 14. Assumed response and path formed by the tube wall under different boundary conditions: (b) inner crushing (i) and (ii), and (c) inner conic crushing (ii).

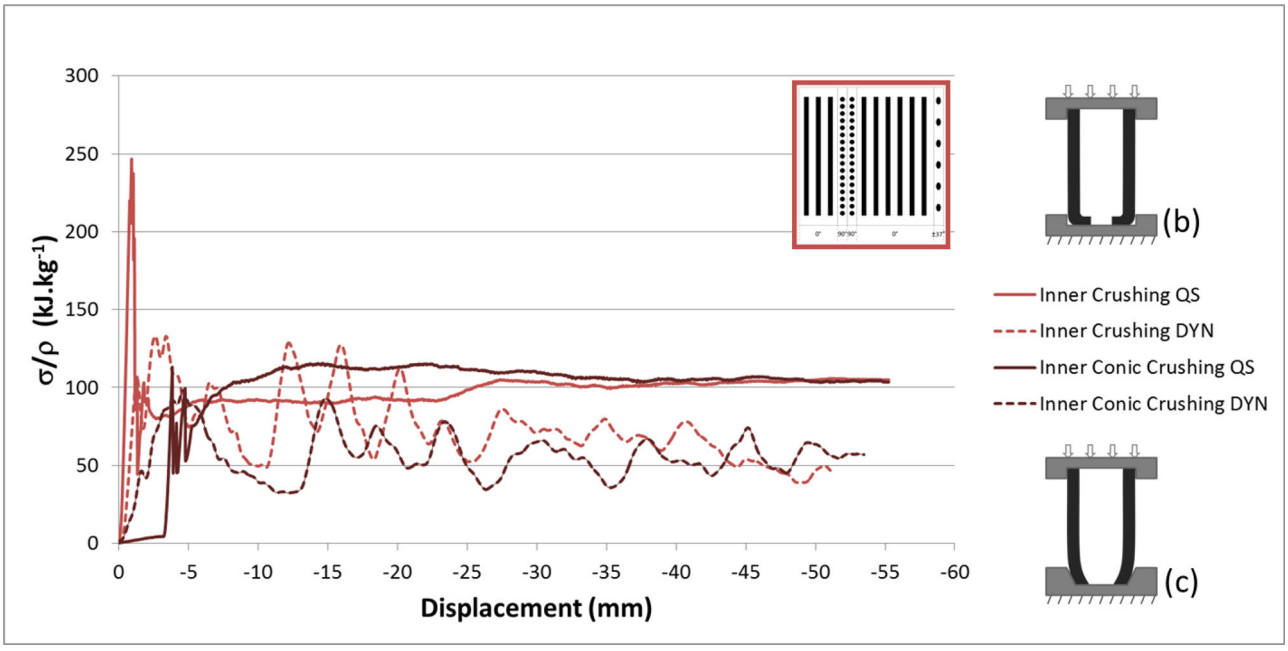

Figure 15. Stress over density/displacement curves for tube sample 2 in configurations (b) and (c).

materials. Examples of dynamic and quasi-static crushing differences are displayed in Figures 13 and 15 for tubes samples 1 and 2 respectively, in configuration (b) and (c).

In case of quasi-static inner crushing confinement (b), a slight but still significant increase of the curve can be noted towards the end, starting at 40 mm. Allegedly, this rise should even be starting sooner, at about 23 mm, distance corresponding to half the tube interior diameter, when the wall bottom end meets at the center of the tube (see Figure 14(b.i)).

This rise is not present for tube specimen 2, the interior ply of which is not woven. Without this woven inner cover, it is suspected that the tube interior walls are less guided and undergo more severe and intense brittle fracture before meeting and densifying at the center of the tube, as compared to tube 1. In that situation, they conceivably lost most of their rigidity and post-testing observations showed that debris were more pushed upwards inside the tube structure than radially inward (see Figure 14(b.ii)). In this instance, since the tube interior walls do not meet, no increase of the stress is observed on the curve, contrary to situation (b.i) (see Figure 14).

An increase of the stress at the end could be beneficial and valuable for a surge in the SEA value: the densification of partially crushed material inside the tubular structure stabilises the crushing process, resulting in an increase of the mean crushing stress and therefore the SEA. Similarly, this increase is not seen for either specimens (1 or 2) in quasi-static for the inner conic crushing, leading to the

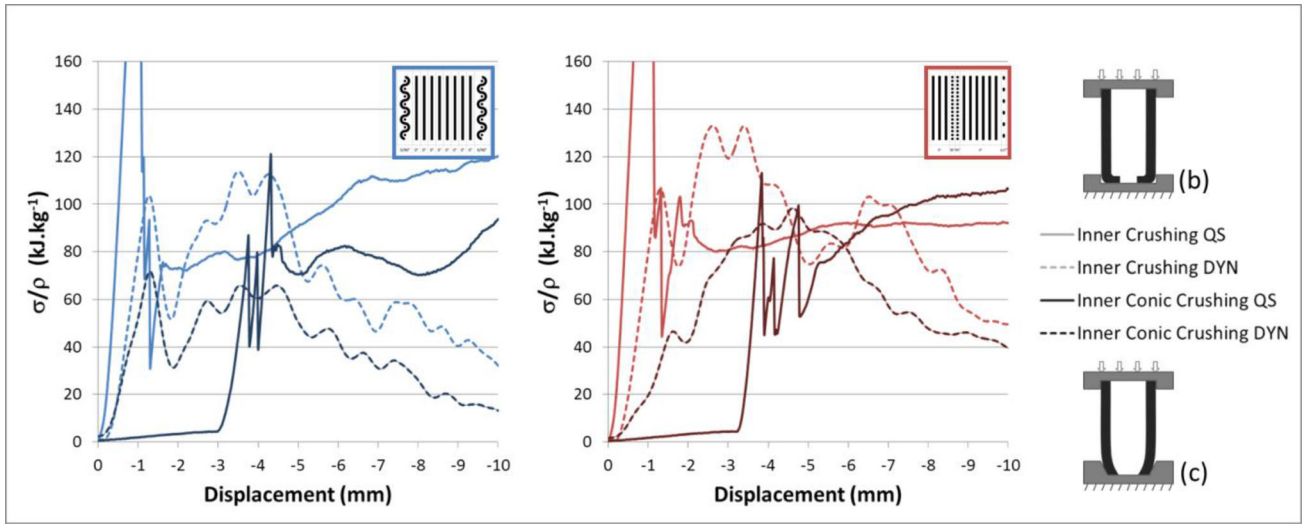

Figure 16. Zoom of stress over density/displacement curves for tube samples 1 and 2 in configurations (b) and (c).

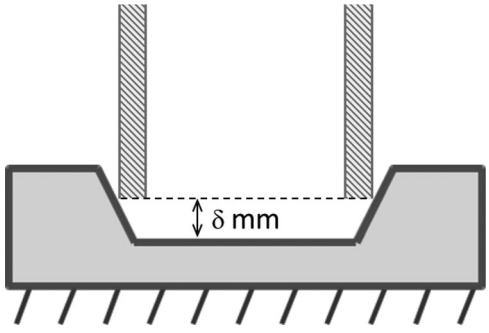

Figure 17. Inner conic part and initial tube position.

assumption that the slope inclination guides the tubes walls on the inside more gradually and curves them more sharply before they meet (see Figure 14(c.ii)).

For quasi-static configuration with a conic initiation (c), compressive hoop stress is first generated, as the inner conic-shaped part constrict the extremity of the tubular structure. Therefore the axial crushing force in the vertical direction takes longer to apply as the exterior diameter of the tubular structure slides along the inner conic slope, before being axially loaded. This setback is incidental to the height of the conic shape (see Figure 17). This can be seen in Figures 13, 15 and 16 for configurations (c) at the very beginning of the curve between 0 and 3 mm displacement.

Due to the important change in velocity magnitude and the dynamic shock resulting from the impact, this delay is not as clearly observed in dynamic trials (see Figures 13 and 15). However a focus on the beginning of the curves (see Figure 16) tends to disclose this progressive and gradual stabilization phase for dynamic cases, mixed up with the oscillations of the signal, especially visible for tube sample 2. For the dynamic tests, this transition phase is almost identical for inner crushing and inner conic crushing (mainly due to friction). This observation may be considered with caution as the filtering is bound to have an impact on the shape of the final curve. However, the trend is similar when the cutoff frequency of the filtering is increased, confirming this assumption.

3.3. Crushing stress

This section relates to the crushing stress of the different tube specimens in the three tested configurations. It aims at explaining the overall crushing behavior through the yield of the structure, given by the crushing peak, and through the mean crushing stress value, corresponding to the behavior of the specimen in crushing.

Figure 18 presents the crushing peak value in both quasi-static and dynamic modes for all tubes samples in all configurations, with the theoretical compressive strength yielding limit (as calculated in Table 6) displayed in the background. Both quasi-static and dynamic crushing peaks in this graph are expressed in stress level (MPa) for a straightforward comparison with the compressive stress (σ_{max}).

According to Figure 18, configuration (b) (inner crushing) is the configuration for which tubes samples are closest to reach their theoretical yielding limit (as can be seen for tubes samples 2, 3, 4 and 5, but except tube sample 1) and in a lesser extent, configuration (a) (free crushing) for tubes sample 3, 4 and 5. In any case, tube sample 1 does not appear to render its full potential, as it stands at about 50% below its theoretical compressive strength. Usually, this initial peak is detrimental, as it introduces a substantial stress drop that converts in a large energy drop.

When comparing the mean crushing stress for all tubes samples in all configurations (see Figure 19), the dynamic effect is clearly visible for tube sample 1, whereas it globally seems less impacting on other samples. It is strongly supposed that as there are more 0°-oriented fibers present in those samples, the overall rupture is mainly due to kink-bands effects, leading to global structure failure. Dynamic effects must be more significant and have a bigger impact on that kind of damage in crushing than on sole matrix rupture in compression. Furthermore, the compressive stress $\sigma_{crushing}$ for

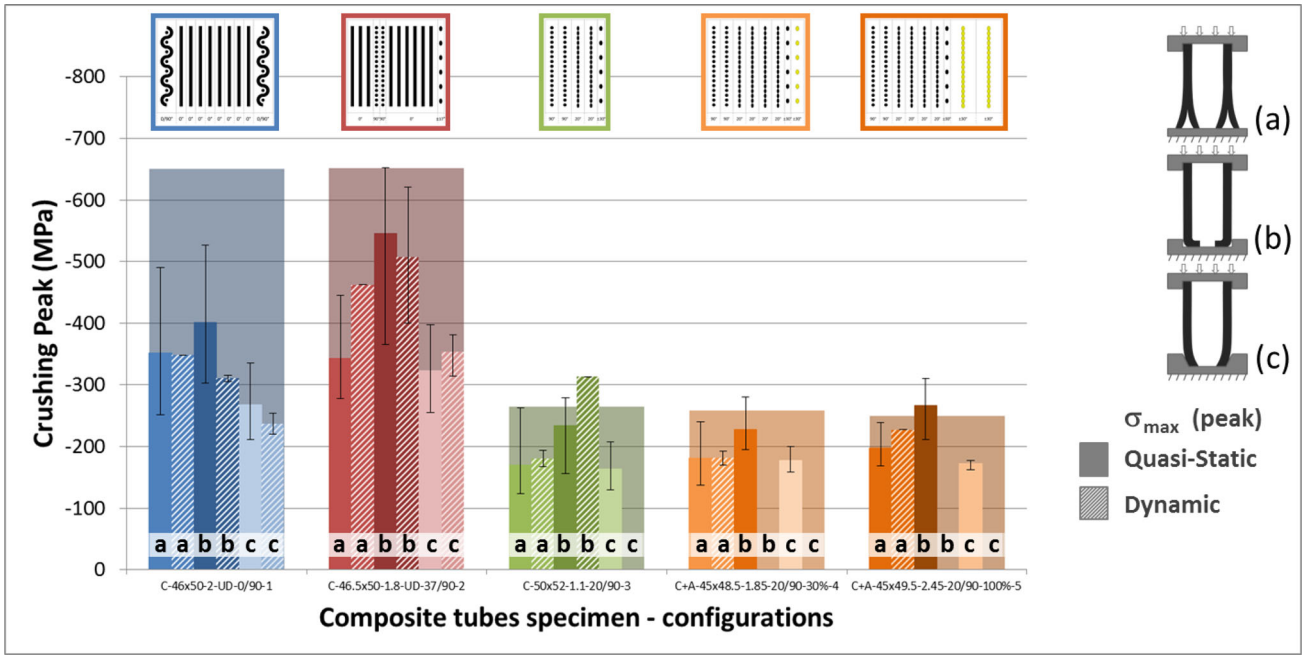

Figure 18. Crushing stress peak (QS and DYN) for tubes 1–5 in configurations (a), (b) and (c).

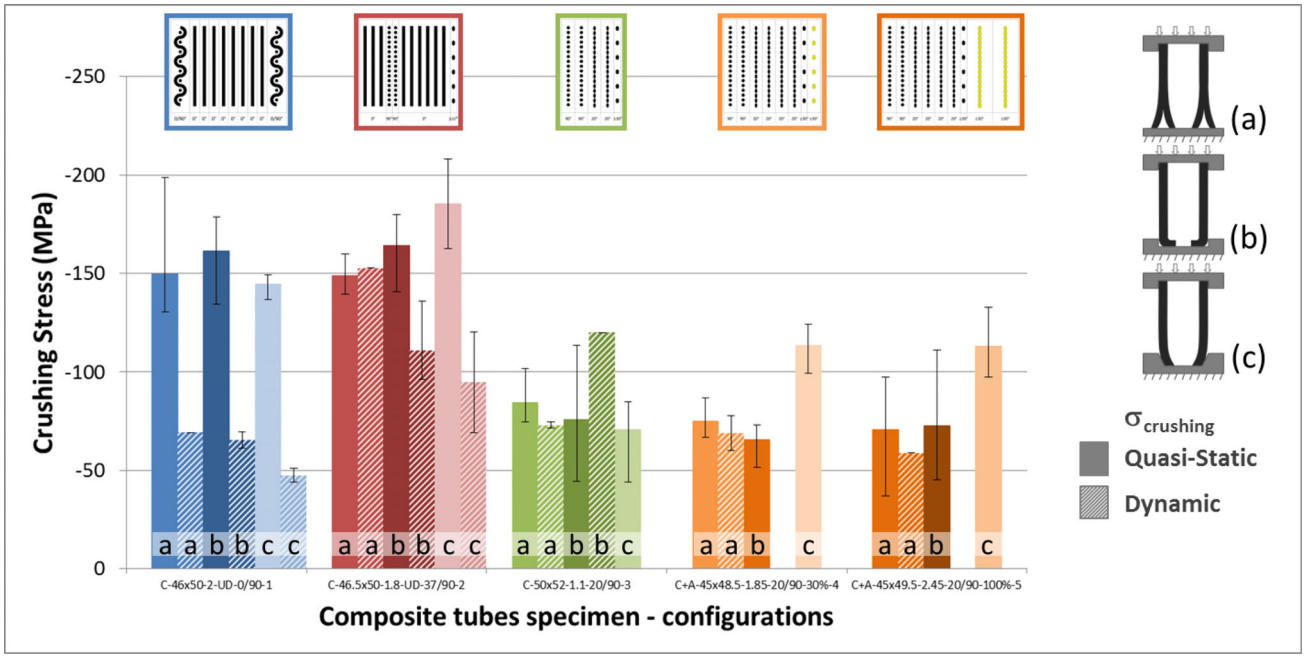

Figure 19. Mean crushing stress (QS and DYN) for tubes 1–5 in configurations (a), (b) and (c).

dynamic loading appears to be higher for samples containing 90°-oriented fibers, than those with mainly 0°-oriented fibers, confirming the low dependence on rate for matrix rupture.

Tubes specimens 4 and 5, which are partially and totally covered with an aramid lay-up on the outer surface, perform relatively fairly, although the aramid fibers rigidity is lesser than the carbon fibers. Their core carbon structure and stratification is very similar to tube specimen 3, which explains their global similar behavior. The major difference therefore lies in the thickness of the tube wall, about half thick for tube specimen 3 compared to other tubes. Tube samples 4 and 5 have not been tested in dynamic crushing for configuration (b) and (c), nor has tube sample 3 in configuration (c) due to a lack of samples at the time.

Crushing stress values clearly show that tube specimen 1 performs very poorly in dynamic crushing, compared to other tubes specimens and also to its own performance in quasi-static crushing.

Overall, in quasi-static loading, the crushing stress always averages around 150 MPa, which approximately corresponds to the matrix rupture stress in compression. In dynamic loading, only tube sample 2 in configuration (a) (free

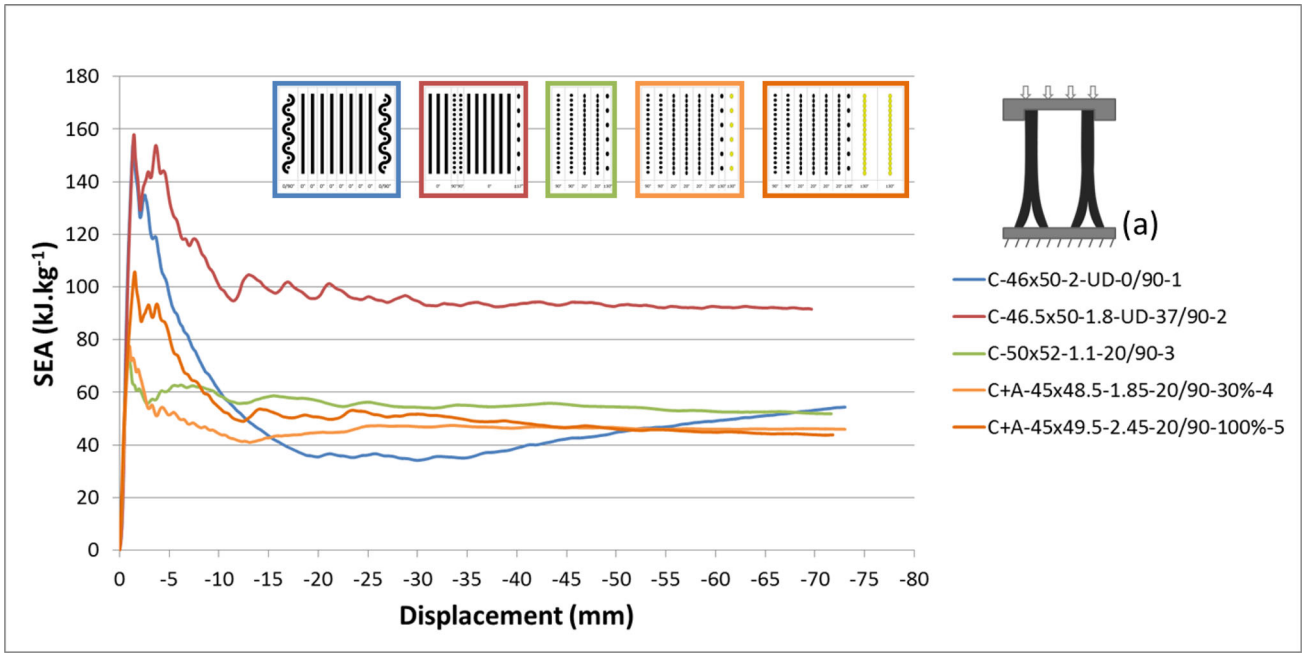

Figure 20. SEA-displacement curve in dynamic loading for tubes 1–5 in free crushing configuration (a).

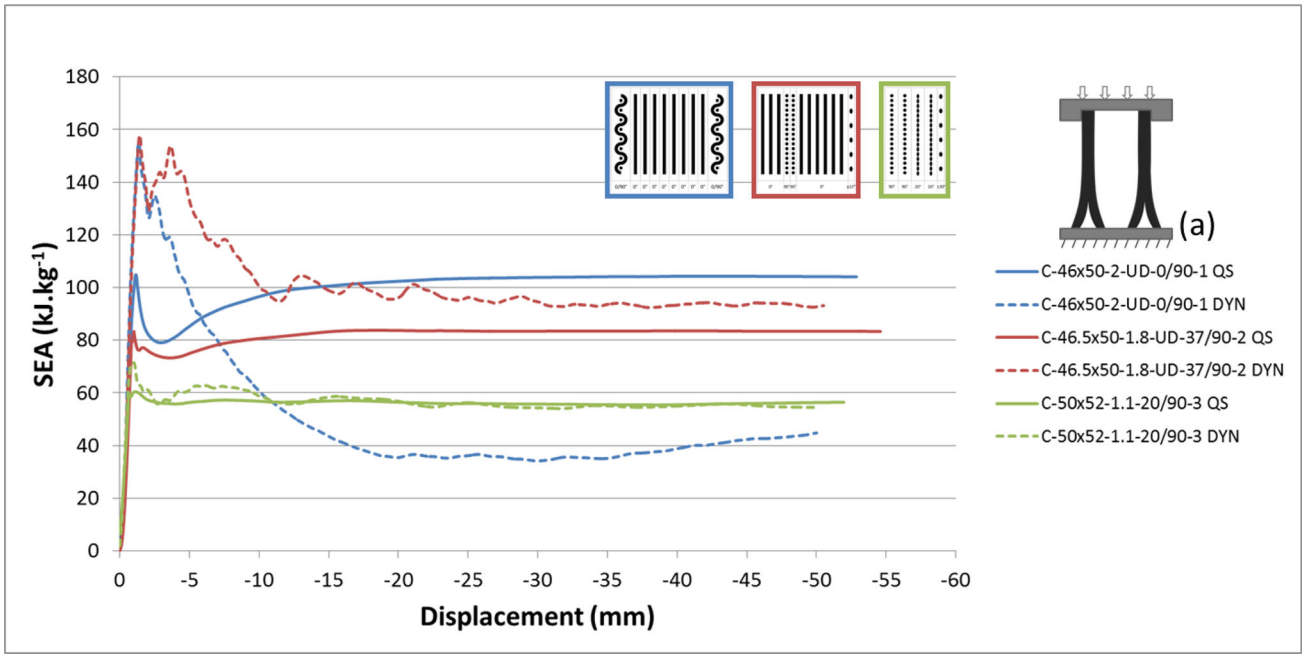

Figure 21. SEA-displacement curve (QS and DYN) for tubes 1–3 in free crushing configuration (a).

crushing) reached 150 MPa. It can therefore be supposed that other configurations ((b) and (c)) have created more brutal ruptures, most particularly due to global and local buckling, since a pure compressive configuration should produce a 150 MPa compressive stress. It can therefore be inferred that both the inner crushing and inner conic crushing configurations destabilise the crushing in dynamic loading.

3.4. Sea evolution

The following discussion, namely Figures 20, 21 and 22 displaying the SEA evolution with the vertical displacement, presents results based on actual SEA values, that is to say calculated using the formula given by Equation (3) and using non-filtered stress values. As the SEA equation is based on an integration, it already acts as a filter, hence the smoothing and difference with the stress/density curves.

The evolution of SEA for tube specimens 1 to 5 in dynamic configuration (a) is presented in Figure 20. From this figure, it is obvious that tube specimen 2 surpasses all other specimens in terms of SEA capacity, despite the fact that its peak load is initially identical to tube specimen 1. That latter specimen performs poorly under dynamic loading, collapsing very easily and quickly.

Compared to quasi-statics, in dynamic crushing, the stabilization phase takes longer: while for quasi-static loading 5

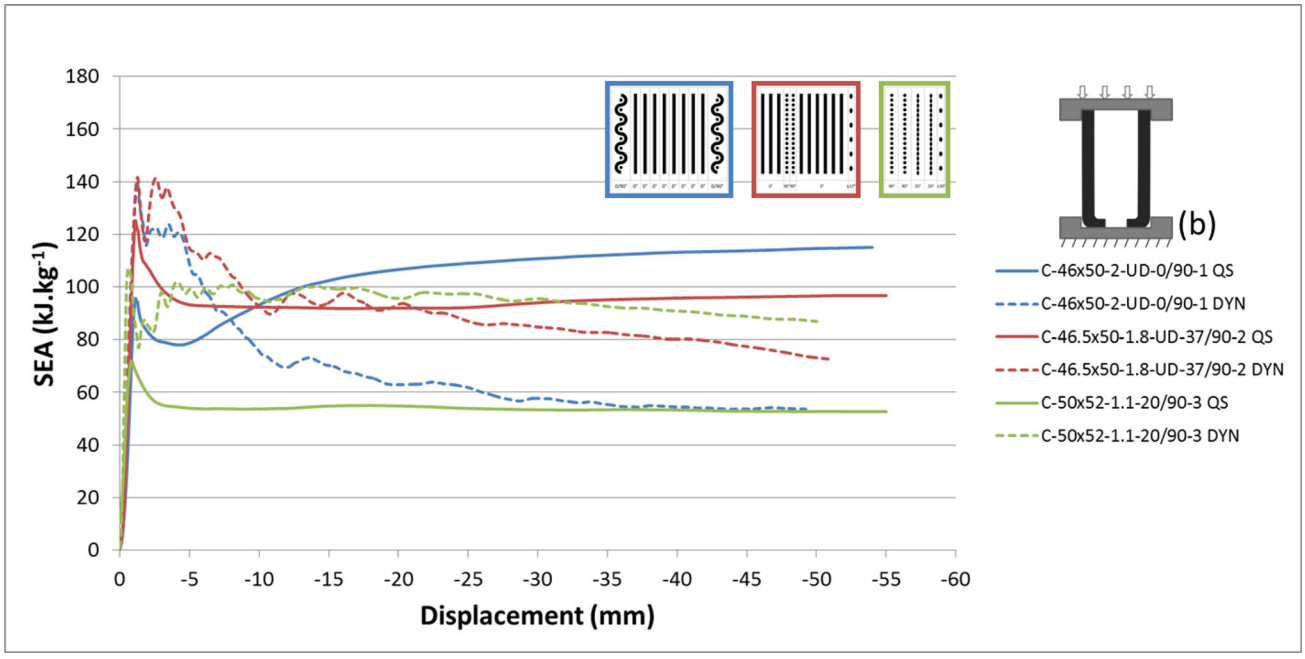

Figure 22. SEA-displacement curve (QS and DYN) for tubes 1–3 in inner crushing configuration (b).

to 10 mm are required, in dynamic cases, it takes 15 to 20 mm approximately. This, as many aspects observed in dynamic mode, can be partially explained by the numerous waves generated during dynamic impact.

For the free crushing (a) and inner crushing (b) configurations, the initial peak is generally higher in dynamics than in quasi-statics (see Figures 21 and 22). This is particularly true for both samples with mainly 0°-oriented fibers (samples 1 and 2), which coincidently have the same peak profile, whether in configuration (a) or (b).

For the inner crushing configuration (configuration (b), see Figure 22), it seems that the evolution of SEA over displacement tends to decrease at the end of the curves for all three dynamic crushing and especially for samples 2 and 3. This does not appear to have any particular reason, a larger number of tests would be required to confirm or correct that tendency.

3.5. Sea and quasi-static/dynamic comparison

Figure 23 summarises the SEA values resulting from experimental testing both in quasi-static and dynamic loading conditions for all three configurations and tube samples 1 to 5 (when available).

Generally SEA values are lower in dynamic crushing than in quasi-static crushing. This finding has also been largely reported in previous studies [13,19,23,33,39,42,46]. Overall, based on values reported in Figure 23, tube specimen 2 performs better in dynamic loading than other tube specimens for all configurations, only matched by tube specimen 3 in inner crushing configuration (b) in dynamic loading. This result is strongly suspected to be the consequence of 90°-oriented fibers present in the core structure of the tubes walls. More specifically, tube specimen 2 presents similar results in dynamic and quasi-static loadings for configuration (a) (free crushing), but shows a relative to moderate decrease in SEA values for configuration (b) and (c): 28% and 42% decrease respectively.

Such similar results differences between dynamic and quasi-static loading for configuration (a) can be observed for specimens 2, 3, 4 and 5, while tube specimen 1 clearly fails for all configurations when dynamically solicited, with a reduction of the SEA value by at least 50% between quasi-static and dynamic conditions, more precisely a reduction of 53% (a), 55% (b) and 61% (c) of the SEA when compared to quasi-static loading.

Problematic issues observed for tube specimen 1 in dynamic loading may come from the too large thickness created by the consecutive 0° plies at the center (see Figure 24), whereas for tube specimen 2, interleaved 90° plies must stabilise the structure and therefore smooth the dynamic rupture.

Tube specimens 3 (mostly 90°-oriented), 4 and 5 (identical 90°-oriented basis with an additional aramid cover) present almost identical results for dynamic and quasi-static loading in free crushing configuration (configuration (a)). It is only slightly higher for the quasi-static rate. This trend has to be confirmed however, as several data points are missing.

However, tube specimen 3 performs better in configuration (b) (inner crushing) for dynamic loading. This can be considered two ways: either a better efficiency in term of energy absorption in dynamic loading in this configuration, or an almost identical effectiveness in quasi-static and dynamic loading when taking into account the margin of error and high dispersion in quasi-static loading. Further testing on a larger number of samples would be required to decisively rule on that trial. With this in consideration, it can presently be stated that in dynamic loading, tube specimen 3 in inner crushing configuration (configuration (b)) achieves similar results as tube specimen 2 in dynamic

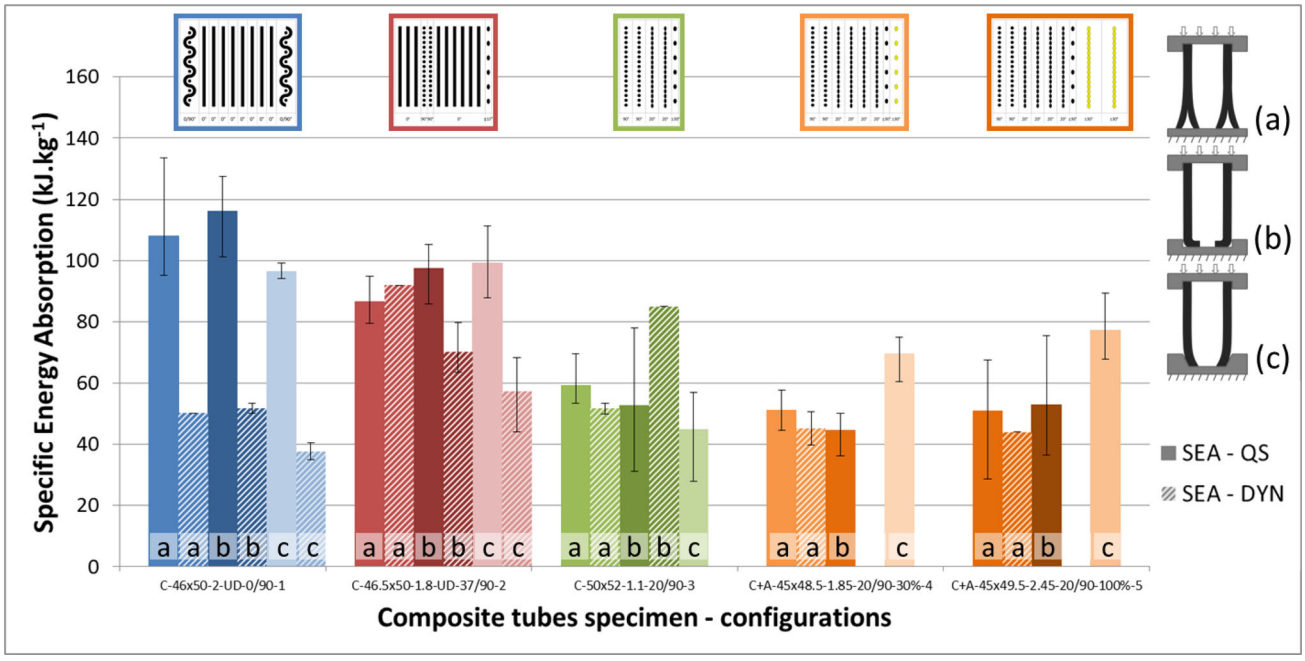

Figure 23. Comparison of (QS and DYN) SEA values for tubes 1–5 in configurations (a), (b), (c).

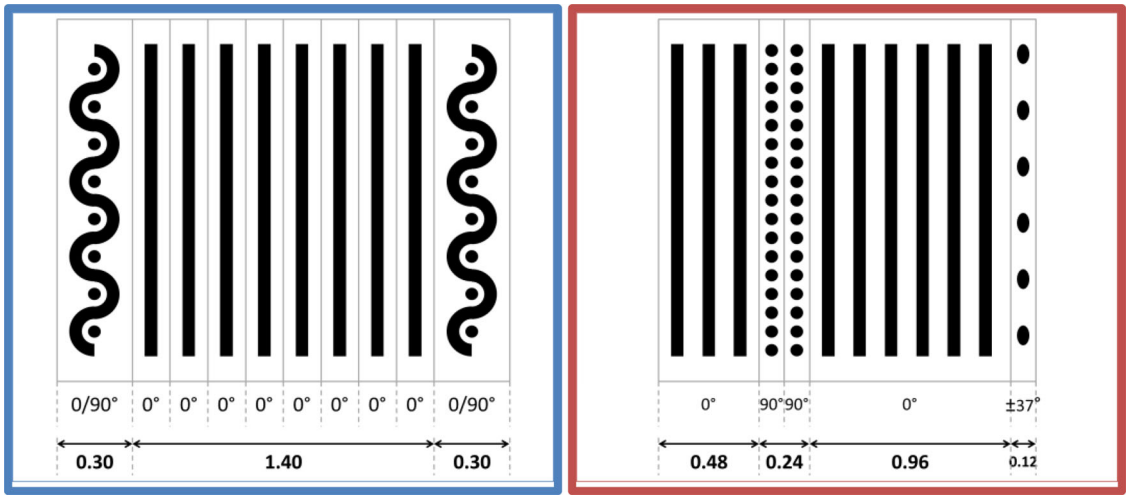

Figure 24. Highlight of the core structure of tube specimen 1 (left) and 2 (right).

loading. Tube 3 in configuration (b) returns higher SEA values than tube 2 in configuration (b) and (c) but they are slightly lower than tube 2 in configuration (a).

Generally, tube specimens with 90°-oriented fibers seem to perform better in dynamic loading. However, overall results and observations lead to the conclusion that in order to have a worthy and strong SEA both in quasi-static and dynamic rates, it is required to have a stratification with 0°-oriented plies stabilised by a woven fabric or by few 90°-oriented plies. It also appears that in dynamic loading it is essential to avoid having too many consecutive 0°-oriented plies in order to prevent catastrophic failures. In dynamic conditions, the presence of 90°-oriented plies that stabilise the structure appears to be a major requirement.

In conclusion, tubes specimens with a partial or total 90°-oriented fibers base structure perform better in dynamic than in quasi-static compared to tubes specimens with a full 0°-oriented fibers base-line structure. This is explained by the structural lay-up order and the thickness of that lay-up.

- Free crushing achieves better for specimen with a mixture of 0° and 90°-oriented fibers base structure (tube 2, configuration (a)).
- Inner crushing achieves better for specimen with a full 90°-oriented fibers base-line structure. (tube 3, configuration (b))

4. Conclusion

Dynamic and quasi-static crushing tests were achieved for different circular hybrid composite tubes samples in various configurations using several trigger initiations. SEA values up to 90 kJ.kg^{-1} were obtained, achieving better than most instances from the literature, averaging around 50 kJ.kg^{-1}

for Carbon/Epoxy laminates. The impact velocity for the dynamic testing was set at $5\,m.s^{-1}$. Specimens with 90°-oriented fibers perpendicularly oriented with the direction of compression reached the highest SEA values while those with mainly 0°-oriented fibers coincidental with the direction of compression performed unwell. It has consequently been established that in dynamic loading, the presence of 90°-oriented fibers stabilised by woven plies greatly enhances the energy dissipation capability of the structure. This was not the case in quasi-static loading, where 0°-oriented specimens achieved best SEA values and met highest expectation in terms of energy dissipation. Moreover, unidirectional laminates oriented at 0° performed 50% lesser between quasi-static and dynamic rates. This has been explained by the too large thickness made by the consecutive 0° plies, yielding by kink-band effect. Incidentally, an inner constrained containment is more effective in most cases, reducing the initial peak load without drastically reducing the SEA value. Inner conic crushing, however, although reducing the initial peak load, also reduces the overall SEA value.

In order to complete this study and provide complementary understanding regarding the dynamic effect in composite tube crushing, it could be interesting to vary the impact speed for the dynamic crushing tests, and especially increase it to high-speed velocity, since all trials in the present study were performed under the same impact velocity and the literature, for the most part, reports a significant effect of the strain rate. A study of the size of the debris and a comparison of their form and size between quasi-static and dynamic testing might provide more insights regarding the fracture and damage mode that undergo the tubular structure during these two load types.

Investigation regarding the D/t ratio (diameter over tallness) of the tubular structures as well as the wall thickness impact on the crushing behavior and crush strength might be helpful. Similarly, a more elaborate study on the cone angle, and sloping inclination of the inner conic configuration might be needed, to best adjust that parameter. Finally, testing of chamfered or notched tubular structure, in combination with the proposed boundary conditions, might help further reduce the peak load and enhance the SEA capacity at the same time.

Disclosure statement

No potential conflict of interest was reported by the authors.

Funding

Financial support for this study was provided thanks to FEDER funds through the joint project SKYSEAT co-funded by ARTEC Aerospace Company, the Occitanie – Pyrénées-Méditerranée Region (ex-Midi-Pyrénées Region) and the ISAE-SUPAERO.

References

[1] Heimbs S, Strobl F, Middendorf P, et al. Composite crash absorber for aircraft fuselage applications. WIT Trans Built Environ. 2010;113:3–14.

[2] Van Beek JAB. Dynamic seat testing and head injury criteria - An aircraft manufacturer's experience and a view on the future. In: Proceedings of the 21st Congress of International Council of the Aeronautical Sciences; 1998 Sep 13–18; Melbourne, Australia.

[3] Olschinka C, Schumacher A, Riedel D. Dynamic simulation of flight passenger seats. In: Proceedings 5, LS-DYNA Anwenderforum; 2006 Oct 12–13; Ulm, Germany.

[4] Abedi MM, Niknejad A, Liaghat GH, et al. Foam-filled grooved tubes with circular cross section under axial compression: an experimental study. Iran J Sci Technol Trans Mech Eng. 2018; 42(4):401–413.

[5] Qaiser Z, Qureshi OM, Johnson S, et al. Thin walled circular tubes with sinusoidal embedded patterns under axial impacts. Thin-Walled Struct. 2016;99:76–82.

[6] Farley GL. Energy absorption of composite materials. J Compos Mater. 1983;17(3):267–279.

[7] Thornton PH. The crush behavior of pultruded tubes at high strain rates. J Compos Mater. 1990;24(6):594–615.

[8] Hamada H, Ramakrishna S, Satoh H. Crushing mechanism of carbon fibre/PEEK composite tubes. Composites. 1995;26(11): 749–755.

[9] Mamalis AG, Robinson M, Manolakos DE, et al. Crashworthy capability of composite material structures. Compos Struct. 1997;37(2):109–134.

[10] Hull D. A unified approach to progressive crushing of fibre-reinforced composite tubes. Compos Sci Technol. 1991;40(4): 377–421.

[11] Pinho ST, Camanho PP, DE Moura MF. Numerical simulation of the crushing process of composite materials. Int J Crashworthiness. 2004;9(3):263–276.

[12] Supian ABM, Sapuan SM, Zuhri MYM, et al. Hybrid reinforced thermoset polymer composite in energy absorption tube application: a review. Defence Technol. 2018;14(4):291–305.

[13] Brighton A, Forrest M, Starbuck M, et al. Strain rate effects on the energy absorption of rapidly manufactured composite tubes. J Compos Mater. 2009;43(20):2183–2200.

[14] Israr HA, Rivallant S, Bouvet C, et al. Finite element simulation of 0°/90° CFRP laminated plates subjected to crushing using a free-face-crushing concept. Compos Part A: Appl Sci Manuf. 2014;62:16–25.

[15] Evans AG, Adler WF. Kinking as a mode of structural degradation in carbon fiber composites. Acta Metall. 1978;26(5): 725–738.

[16] Gutkin R, Pinho ST, Robinson P, et al. A finite fracture mechanics formulation to predict fibre kinking and splitting in CFRP under combined longitudinal compression and in-plane shear. Mech Mater. 2011;43(11):730–739.

[17] Thornton PH, Harwood JJ, Beardmore P. Fiber-reinforced plastic composites for energy absorption purposes. Compos Sci Technol. 1985;24(4):275–298.

[18] Browne AL, Johnson NL, Botkin ME. Composite crash box: roll wrap fabrication and dynamic axial crush performance. In: Proceedings of the ASME 2007 International Mechanical Engineering Congress and Exposition, ASME Digital Collection, Volume 16: Transportation Systems; 2007 Nov 11–15; Seattle, WA; Paper No. IMECE2007-41143. p. 305–312.

[19] Schmueser DW, Wickliffe LE. Impact energy absorption of continuous fiber composite tubes. J Eng Mater Technol. 1987; 109(1):72–77.

[20] Browne AL, Johnson NL. Dynamic axial crush tests of roll wrapped composite tubes: plug vs. non-plug crush initiators. In: Proceedings of the ASME 2005 International Mechanical Engineering Congress and Exposition, Engineering/Technology Management, ASME Digital Collection; 2005 Nov. 5–11; Orlando, FL; Paper No. IMECE. 2005-79158. p. 317–325.

[21] Wang Y, Feng J, Wu J, et al. Effects of fiber orientation and wall thickness on energy absorption characteristics of carbon-reinforced composite tubes under different loading conditions. Compos Struct. 2016;153:356–368.

[22] Muralikannan R, Velmurugan R, Eswaraprasad GL. Energy absorption characteristics of circular composites tubes in quasi static and impact loading. In: Proceedings of the IMPLAST 2010 Conference; 2010 Oct.; Providence, RI: Springer. p. 12–14.

[23] Mamalis AG, Yuan YB, Viegelahn GL. Collapse of thin–wall composite sections subjected to high speed axial loading. Int J Veh Des. 1992;13(5-6):564–519.

[24] Jacob GC, Fellers JF, Simunovic S, et al. Energy absorption in polymer composites for automotive crashworthiness. J Compos Mater. 2002;36(7):813–850.

[25] Xu J, Ma Y, Zhang Q, et al. Crashworthiness of carbon fiber hybrid composite tubes molded by filament winding. Compos Struct. 2016;139:130–140.

[26] Waimer M, Kohlgrüber D, Hachenberg D, et al. Experimental study of CFRP components subjected to dynamic crash loads. Compos Struct. 2013;105:288–299.

[27] Lavoie JA, Kellas S. Dynamic crush tests of energy-absorbing laminated composite plates. Compos Part A: Appl Sci Manuf. 1996;27(6):467–475.

[28] Chiu LNS, Falzon BG, Ruan D, et al. Crush responses of composite cylinder under quasi-static and dynamic loading. Compos Struct. 2015;131:90–98.

[29] Al Galib D, Limam A. Experimental and numerical investigation of static and dynamic axial crushing of circular aluminum tubes. Thin-Walled Struct. 2004;42(8):1103–1137.

[30] Costas M, Díaz J, Romera LE, et al. Static and dynamic axial crushing analysis of car frontal impact hybrid absorbers. Int J Impact Eng. 2013;62:166–181.

[31] Farley GL. The effects of crushing speed on the energy-absorption capability of composite tubes. J Compos Mater. 1991; 25(10):1314–1329.

[32] Farley GL. Relationship between mechanical property and energy-absorption trends for composite tubes. Hampton (VA): Langley Research Center; 1992. (NASA Technical Paper, NASA-TP-3284, 19930007348).

[33] Schultz MR, Hyer MW, Fuchs HP. Static and dynamic energy-absorption capacity of graphite-epoxy tubular specimens. Mech Compos Mater Struct. 2001;8(3):231–247.

[34] Browne AL, Zimmerman KL. Dynamic axial crush of automotive rail-sized composite tubes: part 2 — tubes with braided reinforcements (Carbon, Kevlar®, and Glass) and non-plug crush initiators. In: Proceedings of the ASME 2002 International Mechanical Engineering Congress and Exposition, Transportation: Making Tracks for Tomorrow's Transportation; 2002 Nov. 17–22; New Orleans, LA. Paper No. IMECE2002-32949. p. 69–90.

[35] Okano M, Sugimoto K, Nakai A, et al. Energy absorption properties of braided composite tubes. In: Composite Technologies for 2020, Proceedings of the Fourth Asian–Australasian Conference on Composite Materials (ACCM 4); 2004 Jul.; Sydney, Australia: Woodhead Publishing Limited; p. 466–471.

[36] Mamalis AG, Manolakos DE, Ioannidis MB, et al. On the response of thin-walled CFRP composite tubular components subjected to static and dynamic axial compressive loading: experimental. Compos Struct. 2005;69(4):407–420.

[37] Mamalis AG, Manolakos DE, Ioannidis MB, et al. On the experimental investigation of crash energy absorption in laminate splaying collapse mode of FRP tubular components. Compos Struct. 2005;70(4):413–429.

[38] McGregor CJ, Vaziri R, Xiao X. Finite element modelling of the progressive crushing of braided composite tubes under axial impact. Int J Impact Eng. 2010;37(6):662–672.

[39] David M, Johnson AF, Voggenreiter H. Analysis of crushing response of composite crashworthy structures. Appl Compos Mater. 2013;20(5):773–787.

[40] Murugan R, Ramesh R, Padmanabhan K. Investigation on static and dynamic mechanical properties of epoxy based woven fabric glass/carbon hybrid composite laminates. Procedia Eng. 2014;97:459–468.

[41] Dorival O, Navarro P, Marguet S, et al. Experimental study of impact energy absorption by reinforced braided composite structures: dynamic crushing tests. Compos Part B: Eng. 2015; 78:244–255.

[42] Hu D, Wang Y, Dang L, et al. Energy absorption characteristics of composite tubes with different fibers and matrix under axial quasi-static and impact crushing conditions. J Mech Sci Technol. 2018;32(6):2587–2599.

[43] Tong Y, Xu Y. Improvement of crash energy absorption of 2D braided composite tubes through an innovative chamfer external triggers. Int J Impact Eng. 2018;111:11–20.

[44] Yang Y, Ahmed K, Zhang R, et al. A study on the energy absorption capacity of braided rod composites. Compos Struct. 2018;206:933–940.

[45] Karbhari VM, Haller JE. Rate and architecture effects on progressive crush of braided tubes. Compos Struct. 1998;43(2): 93–108.

[46] McGregor CJ, Vaziri R, Poursartip A, et al. Axial crushing of triaxially braided composite tubes at quasi-static and dynamic rates. Compos Struct. 2016;157:197–206.

[47] Priem C, Othman R, Rozycki P, et al. Experimental investigation of the crash energy absorption of 2.5D-braided thermoplastic composite tubes. Compos Struct. 2014;116:814–826.

[48] Jiménez MA, Miravete A, Larrode E, et al. Effect of trigger geometry on energy absorption in composite profiles. Compos Struct. 2000;48(1–3):107–111.

[49] Hu D, Zhang C, Ma X, et al. Effect of fiber orientation on energy absorption characteristics of glass cloth/epoxy composite tubes under axial quasi-static and impact crushing condition. Compos Part A: Appl Sci Manuf. 2016;90:489–501.

[50] Chambe J-E, Bouvet C, Dorival O, et al. Energy absorption capacity of composite thin-wall circular tubes under axial crushing with different trigger initiations. J Compos Mater. 2020;54(10): 1281–1304.